Structure of the Proteolytic Fragment F34 of Calmodulin in the Absence and Presence of Mastoparan As Revealed by Solution X-ray Scattering†

Yoshinobu Izumi,*,‡ Masayoshi Wakita,§,‖ Hidenori Yoshino,⊥ and Norio Matsushima#

Macromolecular Research Laboratory, Faculty of Engineering, Yamagata University, Yonezawa, Yamagata 992, Japan, Department of Polymer Science, Faculty of Science, Hokkaido University, Sapporo 060, Japan, and Department of Chemistry and School of Allied Health Professions, Sapporo Medical College, Sapporo 060, Japan

Received May 11, 1992; Revised Manuscript Received October 2, 1992

ABSTRACT: The solution X-ray scattering technique has been applied to examine the conformations of the proteolytic fragment F34 (78Asp–148Lys) of calmodulin in the absence of both Ca^{2+} and mastoparan, in the presence of Ca^{2+} only, and in the presence of both Ca^{2+} and mastoparan. The radius of gyration and the molecular weight for the F34 fragment increased by 1.1 ± 0.3 Å and 19%, respectively, upon binding of both 2 mol of Ca^{2+}/mol to the F34 fragment and mastoparan to form the tertiary complex. A smaller change was found for the Ca^{2+}-saturated F34 fragment in the absence of mastoparan (0.3 ± 0.3 Å) without any change of the molecular weight. The analysis based on the small-angle scattering data showed that the F34 fragment in the presence of Ca^{2+} alone preserved the tertiary structure of the globular domain in the crystal to a great extent. Further analyses based on a two-domain model showed that the center-to-center distance between F34 and mastoparan is about 12.7 Å, if the structure of the F34 fragment in the presence of mastoparan resembles that in the absence of mastoparan and if mastoparan in the complex retains an α-helical conformation. The modeling studies using their crystal structure coordinates have been made on the basis of the solution X-ray scattering data. The combined results support a model proposed by Persechini and Kretsinger [Persechini, A., & Kretsinger, R. H. (1988) *J. Cardiovasc. Pharmacol. 12* (*Suppl. 5*), S1–S12], although the center-to-center distance between mastoparan and the F34 fragment is shorter by about 5 Å than that in their model. The shortening is consistent with the model proposed by Strynadka and James [Strynadka, N. C. J., & James, M. N. G. (1990) *Protein: Struct., Funct., Genet. 7*, 234–248].

Calmodulin (CaM)[1] is known to bind several basic, amphiphilic peptides with high affinity (Barnette et al., 1983; Comte et al., 1983; Malencik & Anderson, 1983, 1984). The driving force for this interaction appears to be the induction of an amphiphilic helix in the peptide by the interacting surface in CaM (Cox et al., 1985; McDowell et al., 1985). These amphiphilic peptides are mastoparan (Malencik & Anderson, 1983), mellitin (Comte et al., 1983; Maulet & Cox, 1983), a 27-residue peptide (M13) derived from skeletal muscle myosin light chain kinase (one of the target enzymes) (Klevit et al., 1984), and others (Barnette et al., 1983). These peptides form a tight 1:1 complex with CaM in the presence of Ca^{2+}, and the complex formation enhances the α-helical content of the peptides (Maulet & Cox, 1983; Klevit et al., 1984; McDowell et al., 1985). Since these peptides compete in binding to CaM, both with each other and with the target enzyme such as phosphodiesterase or myosin light chain kinase, the CaM–peptide interaction can be regarded as a good model for that existing between CaM and its target enzymes.

The overall tertiary structure of Ca^{2+}-saturated CaM reveals a dumbbell-shaped molecule with two globular domains (each having Ca^{2+}-binding sites) which are connected by a single long central α-helix (Babu et al., 1985, 1988). A number of studies indicate that CaM undergoes considerable local conformational changes upon binding Ca^{2+}. The increase observed in α-helical content and in exposed hydrophobic surfaces has been implicated in the Ca^{2+}-dependent interactions of CaM with its target enzyme, peptides, and phenothiazine. In these conformational changes of CaM in solution, a question has arisen as to what extent the crystal structure of CaM is held. The SAXS study in the absence of its target peptides showed discrepancies between the solution structure and the crystal structure that if the size and shape of the globular domains are the same in solution as in the crystal, the distances between them must be smaller by several angstroms (Heidorn & Trewhella, 1988).

On the basis of their own results, Persetichini and Kretsinger presented a possible model for the interaction between CaM and M13 complex. They indicated the importance of a flexible structure of the central helix of CaM, and in the formation of the complex, M13 takes an amphiphilic helix. Using different peptides, three independent SAXS groups have revealed that the binding of both Ca^{2+} and an amphiphilic peptide to CaM induces a large change in the tertiary structure of CaM: mastoparan (Izumi et al., 1988; Matsushima et al., 1989), M13 (Heidorn et al., 1989), and mellitin (Kataoka et al., 1989) were used as the peptide. The large conformational change was attributable to a pliable structure of the central helix of CaM. Therefore, these result indicated that the model proposed by Persetichini and Kretsinger (1988) could be

† This work was partly supported by the Terumo Life Science Foundation.

‡ Yamagata University.
§ Hokkaido University.
‖ Present address: Research Institute for Electronic Science, Hokkaido University, Sapporo 060, Japan.
⊥ Department of Chemistry, Sapporo Medical College.
School of Allied Health Professions, Sapporo Medical College.

[1] Abbreviations: CaM, calmodulin; SR, synchrotron radiation; SOXS, solution X-ray scattering, which is the sum of SAXS plus MAXS; SAXS, small-angle X-ray scattering; MAXS, moderate-angle X-ray scattering; R_0, radius of gyration; NMR, nuclear magnetic resonance; CD, circular dichroism.

0006-2960/92/0431-12266$03.00/0

regarded as a starting point of the model of the CaM–peptide complex.

The above SAXS results have been analyzed under the assumption that the size and the overall shape of the globular domains are the same in Ca^{2+}–CaM–mastoparan as in CaM or the Ca^{2+}–CaM complex, and, furthermore, the conformation of the peptide was almost neglected. The tertiary structures and Ca^{2+}-binding properties of the two domains of CaM are conserved almost completly in the fragments of CaM, F12 and F34, respectively, which can be liberated by tryptic digestion (Ikura et al., 1984; Minowa & Yagi, 1984). Therefore, one can use these fragments to investigate the properties of the two domains of CaM.

The purpose of the present paper is to investigate the solution structures of the CaM fragments with or without mastoparan and to present a possible molecular model for the interaction of mastoparan with the fragments. Mastoparan was used as one of the peptides, because it forms a tight 1:1 complex with F34 as well as CaM (Malencik & Anderson, 1984). The high quality of the SOXS data enabled us to present a possible model about the solution structures for the fragments, mastoparan, and the fragment–mastoparan complex. This structural information provides further verification of the previous SOXS results for the solution structures of the Ca^{2+}–CaM–mastoparan complex.

MATERIALS AND METHODS

Sample Preparation. CaM was prepared from pig brain by the method of Yazawa et al. (1980). The tryptic fragments F12 (1Ala–75Lys) and F34 (78Asp–148Lys) were prepared according to the method of Minowa and Yagi (1984). The purity of these fragments was examined by polyacrylamide gel electrophoresis in alkaline urea, and their concentrations were determined by measuring the weight of lyophilized samples and checked by the method of Lowry et al. (1951). Mastoparan was purchased from Peptide Institute Co. (Osaka, Japan) and used after an adjustment of the pH of the solution. The details of the sample preparation are given elsewhere (Yoshino et al., 1989).

For the SOXS measurements, F34 fragment in the absence of Ca^{2+} (Ca^{2+}-free), F34 fragment in the presence of 2.5 mol of Ca^{2+}/mol of fragment (Ca^{2+}-saturated), and the mixture of mastoparan and 2 mol of Ca^{2+}/mol of F34 fragment at a 1:1 molar ratio were prepared in 50 mM Tris-HCl and 120 mM NaCl at pH 7.6. To prepare Ca^{2+}-saturated samples, a 0.1 M $CaCl_2$ solution was added, while to prepare Ca^{2+}-free samples, 0.1 M EDTA was added to 1 mM in final solution. On the other hand, F12 fragment was prepared at only one concentration of the fragment, because of its paucity.

X-ray Scattering Measurements. The SOXS profiles for fragments were recorded with SR from the 2.5-GeV storage ring at the Photon Factory of the National Laboratory for High Energy Physics, Tsukuba, using SOXS optics. The X-ray beam line is equipped with a torroidal focusing mirror and a double-crystal monochromator. The monochromatization was achieved by using silicon (111) reflection. The wavelength of the X-ray was 1.488 Å. Data were recorded using a one-dimensional position-sensitive proportional detector with delay line readout. Corrections for the slit-smearing effect were not made, because quasi-point-type optics were used. The details of the optics and instruments are given elsewhere (Ueki et al., 1983, 1985).

The samples were contained in a quartz cell of 70-μL volume, and the temperature was maintained at 25.0 ± 0.1 °C by circulating water through the sample holder. The scale of the reciprocal parameter, s, equal to $(2 \sin \theta)/\lambda$, was calibrated by observation of the peak from dried chicken collagen, where 2θ is the scattering angle and λ is the X-ray wavelength. The SOXS measurements are composed of both the small-angle X-ray scattering (SAXS) and the moderate-angle X-ray scattering (MAXS) measurements. Exposure time to samples was 600 s for SAXS and 1200 s for MAXS. Irradiation of fragments for periods up to 2400 s produced no change in the scattering profiles.

The SAXS measurements were carried out over the concentration range of 10–25 mg/mL for F34, while the MAXS measurements were carried out only at one concentration of 25.5 mg/mL for the F34 fragment. The corresponding measurements for F12 were made at one concentration of the fragment and therefore have only a preliminary meaning, and the results are not shown until the detailed measurements are made.

The data were analyzed using a HITAC M682H computer of the Computer Center of Hokkaido University and a PC-9801RX personal computer (NEC Co. Ltd.).

Scattering Data Analysis. The inner parts of the scattering profiles, $I(s,c)$, measured as a function of s, in a dilute solution (the protein concentration c is usually expressed in grams per cubic centimeter), were analyzed with the Guinier equation (Guinier & Fournet, 1955):

$$I(s,c) = I(0,c) \exp\{-4\pi^2 R_a(c)^2 s^2/3\} \quad (1)$$

Here $I(0,c)$ is the scattering intensity at $s = 0$ and $R_a(c)$ is the apparent radius of gyration at a finite concentration. In the dilute limit, $I(0,c)$ may be written by

$$Kc/I(0,c) = 1/M + 2A_2c + \ldots \quad (2)$$

where K is a constant, M is the molecular weight of the protein, and A_2 is the second virial coefficient. The constant K was determined by using a series of concentrations of bovine serum albumin as a standard sample (Glatter & Kratky, 1982). In the dilute limit, $R_a(c)$ may be written by

$$R_a(c)^2 = R_0^2 - B_{if.}c + \ldots \quad (3)$$

where R_0 is the radius of gyration at infinite dilution and $B_{if.}$ is the parameter of interparticle interference. Using eq 2 and 3, we can estimate the four parameters M, A_2, R_0, and $B_{if.}$. For the analysis of eq 2 and 3, the range of 10^4 s^2 Å^{-2} was 0.25–2.0 for all samples measured.

The inner parts containing the Guinier region in the scattering profiles were analyzed with the scattering function of a prolate ellipsoid of rotation with semiaxes a, a, and va (Guinier & Fournet, 1955):

$$\int \phi^2\{sa\sqrt{[1 + x^2(v^2 - 1)]}\}\, dx \quad (4)$$

where $\phi^2(sr)$ is the scattering function for a uniform sphere of radius r:

$$\phi^2(sr) = 9\{[\sin(sr) - sr\cos(sr)]/(sr)^3\}^2 \quad (5)$$

For the analysis by eq 4 and 5, the range of 10^2 s Å^{-1} was 0.5–3.0 for all samples measured.

Model Calculations. The overall scattering profiles, $i(s)$, for fragment F34 and the complex can be calculated semi-analytically using a computer program which uses Debye's formula (Debye, 1915):

$$i(s) = \sum\sum f_i f_k \sin(2\pi s r_{ik})/2\pi s r_{ik} \quad (6)$$

where f_i is the form factor for subunit i and r_{ik} is the distance between subunits i and k. Regarding α-carbon as a spherical

subunit, one can calculate the scattering profile and obtain a qualitative scattering profile (Glatter & Kratky, 1982). As a result, comparison between the experimental and calculated profiles is possible. We used the coordinates of the α-carbon positions as determined from the crystal structure (Babu et al., 1988). The coordinates of the F34 fragment were created from 78Asp to 147Ala. The contribution from 148Lys in F34 was omitted, because the coordinate in the crystal structure has not been determined. In building the model of the fragment–mastoparan complex, based on the present SOXS results, we assumed explicitly that mastoparan in the complex retains an α-helical conformation and each fragment retains the corresponding part of the crystal structure of CaM even in the presence of mastoparan. The coordinates of mastoparan were created from those of a standard α-helix with $\phi = -57°$ and $\psi = -47°$. Furthermore, the corresponding part of the model proposed by Persechini and Kretsinger (1988) for the interaction of CaM and M13 was selected as a starting point of the model for the CaM fragment and mastoparan. Their model was modified in order to satisfy the experimental SOXS results. First we changed the center-to-center distance between F34 and mastoparan without changing their relative arrangement. Second, the relative arrangement was changed by rotating and tilting mastoparan to the F34 fragment. The effect of solvent appeared in the scattering at larger angles. By taking correctly into account the effect, it is possible to compare the experimental profile with the calculated profile quantitatively. This requires the exact determination of the volume of the protein inaccessible to the solvent. In the present model calculation, however, we neglected any effect of solvents. Therefore, qualitative comparison between the experimental and calculated profiles is meaningful.

RESULTS

Guinier Region of the Scattering Profile. Examples of Guinier plots for the F34 fragment over the concentration series are shown in Figure 1. In all of the samples studied here, there is no evidence of any upward curvature at low s values in the Guinier plots which could result from aggregation of the samples. The values of $c/I(0,c)$ obtained from the intercepts of the Guinier plots are shown as a function of fragment concentration in Figure 2. Plots in Figure 2 are also linear over the entire concentration range, and the values of $I(0)$ extrapolated to infinite dilution for F34 fragments under different conditions have the molecular weight appropriate for the soluble monomer. The molecular weights M and the second virial coefficients A_2 were calculated using eq 2 and compiled in Table I. The value of M increases about 19% in the presence of both 2 mol of Ca^{2+} and 1 mol of mastoparan, whose increment just corresponds to the molecular weight of both 2 mol of Ca^{2+} and 1 mol of mastoparan, while the values of A_2 are almost constant irrespective of the absence or the presence of mastoparan. Furthermore, these values of M in Table I agree closely with the corresponding values derived from the amino acid sequence. The result for the molecular weight suggests that a complex is formed between the fragment and mastoparan.

Apparent radii of gyration were calculated from the slopes of the Guinier plots using eq 1 and are shown as a function of fragment concentration in Figure 3. The linear increase with decreasing protein concentration was observed in the absence of mastoparan, while the reverse tendency was observed in the presence of mastoparan. The slopes of these lines, which arise from interparticle interference effects, represent a virial coefficient (Guinier & Fournet, 1955).

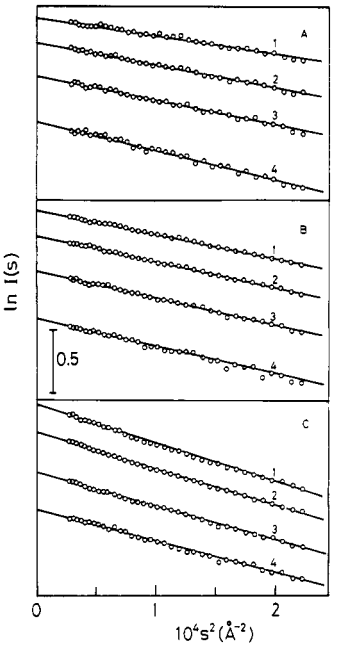

FIGURE 1: Guinier plots for the observed small-angle scattering for the F34 fragment at a series of protein concentrations at pH 7.6. (A) Scattering curves for F34 in the absence of both Ca^{2+} and mastoparan. (B) Curves for F34 in the presence of 2.5 mol of Ca^{2+}/mol of fragment. (C) Curves for F34 in the presence of both 2 mol of Ca^{2+}/mol of fragment and 1 mol of mastoparan/mol of fragment. (1) 25.2 mg/mL; (2) 19.7 mg/mL; (3) 14.3 mg/mL; (4) 9.86 mg/mL.

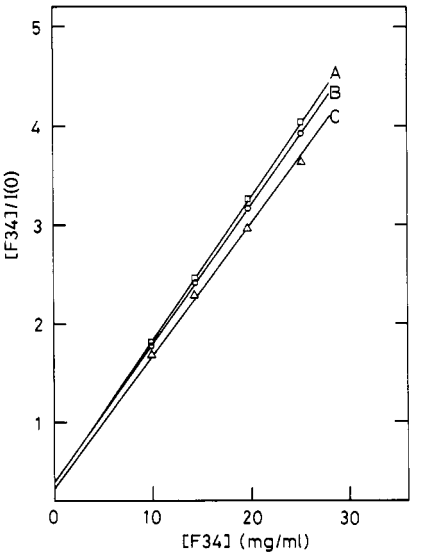

FIGURE 2: Fragment concentration dependence of $c/I(0)$ measured at pH 7.6. The measured $c/I(0)$ as a function of fragment concentration is plotted for F34 fragment (A) in the absence of both Ca^{2+} and mastoparan, (B) in the presence of 2.5 mol of Ca^{2+}/mol of fragment, and (C) in the presence of both 2 mol of Ca^{2+}/mol of fragment and 1 mol of mastoparan/mol of fragment.

Table I compiles the values of the radius of gyration extrapolated to zero fragment concentration and of interparticle interference. The formation of a tertiary complex with Ca^{2+} and mastoparan increases the radius of gyration of the fragment by 1.1 ± 0.3 Å and the molecular weight by about 19% in comparison with that of the Ca^{2+}-free fragment. Furthermore, the formation of the tertiary complex drastically changes the parameter of interparticle interference to a negative value from the positive value in the case of the Ca^{2+}-free fragment. On the other hand, the addition of Ca^{2+} alone hardly changes the values of R_0, M, and A_2 but does change the value of B_{if}.

Table I: Molecular Weight (M) and Second Virial Coefficient (A_2), Radius of Gyration at Infinite Dilution (R_0), and $B_{if.}$ Coefficient for Fragment F34 at pH 7.6[a]

	$10^{-3}M$	10^2A_2 (mol·mL/g^2)	R_0 (Å)	$10^{13}B_{if.}$ (cm^5/g)
F34 fragment in absence of Ca^{2+} and mastoparan	8.25 ± 0.50	2.3 ± 0.2	13.2 ± 0.3	2.9 ± 0.1
F34 fragment in presence of 2.5 mol of Ca^{2+}/mol of fragment	8.25 ± 0.50	2.2 ± 0.2	13.5 ± 0.3	1.5 ± 0.1
F34 fragment in presence of 2.0 mol of Ca^{2+}/mol of fragment and 1 mol of mastoparan/mol of fragment	9.82 ± 0.70	2.2 ± 0.2	14.3 ± 0.3	−3.6 ± 0.1

[a] The definitions of M, A_2, R_0, and $B_{if.}$ are given in the text (eq 2 and 3).

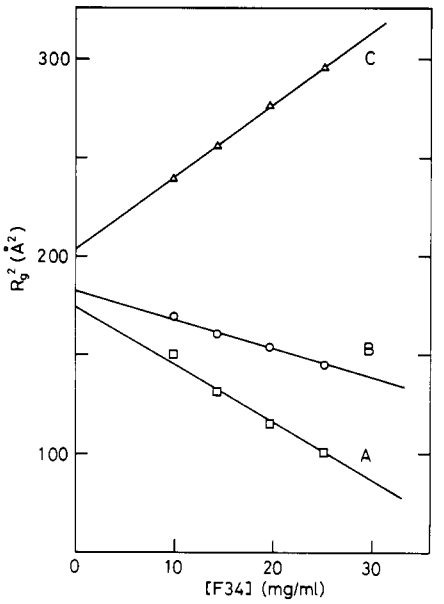

FIGURE 3: Fragment concentration dependence of the measured radius of gyration at pH 7.6. The measured radius of gyration as a function of fragment concentration is plotted for the F34 fragment (A) in the absence of both Ca^{2+} and mastoparan, (B) in the presence of 2.5 mol of Ca^{2+}/mol of fragment, and (C) in the presence of both 2 mol of Ca^{2+}/mol of fragment and 1 mol of mastoparan/mol of fragment.

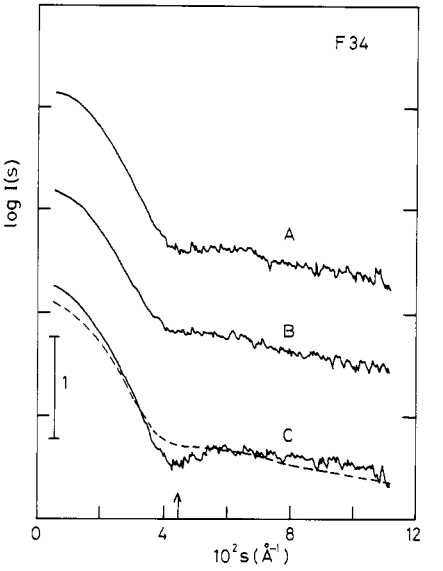

FIGURE 4: Experimental solution X-ray scattering profiles for the proteolytic fragment F34 at 25.5 mg/mL. (A) Experimental profile in the absence of both Ca^{2+} and mastoparan. (B) Experimental profile in the presence of 2.5 mol of Ca^{2+}/mol of fragment. (C) Experimental profile in the presence of both 2 mol of Ca^{2+}/mol of fragment and 1 mol of mastoparan/mol of fragment. For clarity, the ordinate under different conditions has been separated by 1.0 unit. The dashed line of trace C is the sketch of trace B.

Inner Part of the Scattering Profile Outside the Guinier Region. Using eq 4 and 5, the semiaxis (a) and the axial ratio (v) for the F34 fragment in the presence of 2.5 mol of Ca^{2+}/mol of fragment are estimated as a(Å) = 13.2 ± 0.3 and v = 1.8 ± 0.1, while the corresponding values of the C-domain in the crystal structure of intact CaM are a(Å) = 12.9 and v = 1.6, respectively, whose values were cited from the paper of Heidorn and Trewhella (1988). These results indicate that the semiaxis and the axial ratio for the F34 fragment in solution are almost comparable to those of the C-domain in the crystal structure of intact CaM.

Outer Part of the Scattering Profile. Figure 4 shows the MAXS profiles for the F34 fragment. The MAXS profile for the Ca^{2+}-free fragment is characterized by the presence of a single broad maximum near s = 0 and a broad maximum near s = 0.06. Upon binding Ca^{2+}, the changes in the MAXS profile consist of a slight change in the profile of the F34 fragment. On the other hand, upon binding mastoparan, the MAXS profile of the Ca^{2+}-saturated F34 fragment differs remarkably from those of Ca^{2+}-free and/or Ca^{2+}-saturated F34 fragment in the absence of mastoparan. A prominent decrease of the minimum near s = 0.045 Å^{-1} was observed for the Ca^{2+}-saturated fragment–mastoparan complex.

DISCUSSION

The results of the SAXS measurements presented here show that the values of M, A_2, and R_0, except for the value of $B_{if.}$, for the F34 fragment in the absence of mastoparan are hardly changed upon binding Ca^{2+} and that the semiaxis and the axial ratio for the F34 fragment are also almost comparable to those of the C-domain in the crystal structure of CaM. These results suggest that the F34 fragment in the absence of mastoparan consists of a globular domain maintaining most of the tertiary structure of the domain of intact CaM. Furthermore, the most likely reason for the decrease of the value of $B_{if.}$ upon binding Ca^{2+} is the resultant loss of net negative charge of the F34 fragment.

On the other hand, the values of M and R_0 for the F34 fragment in the absence of mastoparan increase upon binding Ca^{2+} and mastoparan. The most straightforward interpretation of the increase of M and R_0 is that a complex is created between the F34 fragment and mastoparan upon binding 1 mol of mastoparan. The formation of the complex is also characterized by the drastic change of the value of $B_{if.}$. The difference of signs means that the interparticle interference effect in the absence of mastoparan is totally changed from that in the presence of mastoparan and suggests the formation of the complex.

In order to present molecular explanation for the changes of these parameters in F34 upon binding Ca^{2+} and mastoparan, two facts are particularly useful. First, the structure of the complex consists of two quite separate but compact globular domains, and, second, its radius of gyration is increased upon binding Ca^{2+} and mastoparan. The first point implies that the radius of gyration of the complex, R_0, making no

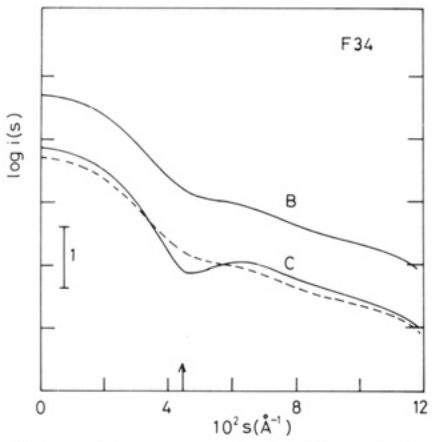

FIGURE 5: Solution X-ray scattering profiles calculated for the proteolytic fragment F34. (B) Calculated model in the presence of 2 mol of Ca^{2+}/mol of fragment. (C) Calculated model in the presence of both 2 mol of Ca^{2+}/mol of fragment and 1 mol of matoparan/mol of fragment. For clarity, the ordinate under two different conditions has been separated by 1.0 unit. The dashed line of trace C is the sketch of trace B.

assumption about shape (Goldstein, 1962), is

$$R_0^2 = (M_{F34}R_{F34}^2 + M_M R_M^2)/(M_{F34} + M_M) + L_{F34M}^2/4 \quad (7)$$

where M_{F34}, M_M, R_{F34}, and R_M are the molecular weights and the radii of gyration of F34 and mastoparan, respectively, and L_{F34M} is the center-to-center distance between F34 and mastoparan.

This analysis based on eq 7 explicitly assumed that the structure of the F34 fragment in the presence of mastoparan resembles that in the absence of mastoparan. Then, from eq 7, L_{F34M} is calculated using the values of R_0 and R_{F34} observed here and assuming R_M = 7.6 Å, where mastoparan in the resolution of this s range may be taken as a cylinder whose radius is about 7 Å and height is about 20 Å. Here M_{F34} and M_M were evaluated from these primary structures. The value of L_{F34M} is about 12.7 Å. The value is drastically small compared with the simple addition between R_{F34} and R_M (ca. 20.8 Å). This fact suggests that the binding site in the F34 fragment is very limited to mastoparan and the complex formation could be made by a specific arrangement between them. As suggested from the model of Persetichini and Kretsinger, the hydrophobic region of mastoparan may interact with a hydrophobic part of the fragment exposed by Ca^{2+} binding. Furthermore, it is noted that this estimated L_{F34M} value corresponds to the half of the center-to-center distance (L_{DD}) between two domains of intact CaM. The present estimation may be reasonable, because it is suggested that the distance L_{F12M} between F12 and mastoparan almost equals that of L_{F34M}, as seen from our previous result in which the value of $L_{DD}/2$ is about 12.5 Å in the presence of both mastoparan and 4 Ca^{2+} ions (Izumi et al., 1989, 1990). Therefore, the present result is consistent with our previous result for the intact CaM–mastoparan complex.

In order to present a more detailed molecular model for the structure of the complex, we calculated the scattering profiles for F34 and its complex using eq 6. Figure 5 shows theoretical SOXS profiles for the F34 fragment in the presence of Ca^{2+} and in the presence of both Ca^{2+} and mastoparan. The scattering profile calculated for F34 with or without mastoparan is very similar to the corresponding MAXS profile shown in Figure 4. That is, the theoretical profile for F34 without mastoparan shows a minimum, a maximum, and another minimum at s = 0.05, 0.06, and 0.08 $Å^{-1}$, respectively. Upon

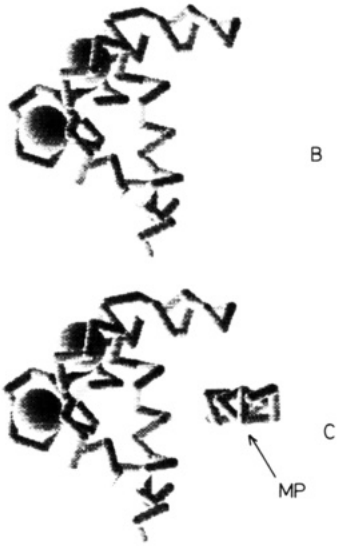

FIGURE 6: α-Carbon traces for the F34 fragment and the complex with mastoparan, in which the two calcium ions are represented by spheres and mastoparan by an α-helix. (B) α-Carbon traces for the F34 fragment which give trace B in Figure 5. (C) α-Carbon traces for the complex of F34 fragment and mastoparan, which give trace C in Figure 5.

binding mastoparan, the theoretical profile also shows a prominent minimum near s = 0.045 $Å^{-1}$. In Figure 6 are shown the α-carbon traces for the F34 fragment and the complex with mastoparan that give the theoretical scattering profiles shown in Figure 5.

The above discussions suggest that the F34 fragment in solution consists of a globular domain maintaining most of the tertiary structure of intact CaM, even in the presence of mastoparan. This is consistent with the results of many studies including NMR, CD, and fluorescence (Minowa & Yagi, 1984; Drabikowski et al., 1982; Dalgarno et al., 1984; Klevit et al., 1984; Ikura et al., 1984; Aulabaugh et al., 1984).

The combined results of the radius of gyration and profile analyses containing both SAXS and MAXS for F34 with mastoparan are well explained in terms of formation of a complex between F34 and mastoparan. This is consistent with earlier results of fluorescence and CD spectra.

The model proposed for the Ca^{2+}–mastoparan–F34 complex is one of the most likely models. Such a model is based on the model for the interaction of CaM and M13 proposed by Persechini and Kretsinger (1988). On the basis of the present SOXS result, however, it is concluded that the center-to-center distance between fragment F34 and mastoparan was shorter by about 5 Å than the corresponding separation in their model. The shortening is consistent with the model proposed by Strynadka and James (1990). From the proposed model, furthermore, it may also be concluded that the MAXS profile with a prominent minimum near s = 0.045 A^{-1} appears in a model requirining that mastoparan has an α-helix structure in the complexed state and that mastoparan interacts with the hydrophobic patch of F34. Difference CD suggested that binding mastoparan to F34 is associated with the induction of a considerable degree of helicity in mastoparan (Higashimjima et al., 1983; Malencik & Anderson, 1984; Sanyal et al., 1988). The present study provides evidence of an induced helix structure for complexed mastoparan.

In conclusion, combining the SOXS technique with model calculations based on the atomic coordinates of the corresponding crystal structure has enabled a clarification of the conformation of mastoparan in the complex as well as that of the complex as a whole.

ACKNOWLEDGMENT

We are grateful to Dr. T. Ueki of the Institute of Physical and Chemical Research, Prof. Y. Miyake, Mrs. T. Matsuo, and S. Nishikida of Hokkaido University, and Prof. O. Minari, Prof. Kanoh, and Dr. A. Abe of Sapporo Medical College for their support of this work and to Dr. K. Kobayashi of the Photon Factory and other members for their help in the experiments of SOXS at the Photon Factory. We thank Prof. K. Yagi and Prof. K. Hikichi of Hokkaido University for useful discussions. The model calculation was carried out by Mr. H. Kawasaki of Hokkaido University and Mrs. N. Yako and H. Sato of Yamagata University. The MODRAST-E (Molecular Display for Raster Graphics, Extended, which was written by Prof. H. Nakano of Himeji Institute of Technology) was used as the molecular graphics. The atomic positions of α-carbons in intact CaM were taken from the Protein Data Bank of Brookhaven National Laboratory, available through the Crystallographic Research Center, Institute for Protein Research, Osaka University. This work has been performed under the approval of the Photon Factory Advisory Committee (Proposal No. 89-047).

REFERENCES

Aulabaugh, A., Niemczura, W. P., & Gibboms, W. A. (1984) *Biochem. Biophys. Res. Commun. 118*, 225–232.

Babu, Y. S., Sack, J. S., Greenhough, T. J., Bugg, C. E., Means, A. R., & Cook, W. J. (1985) *Nature 315*, 37–40.

Babu, Y. S., Bugg, C. E., & Cook, W. J. (1988) *J. Mol. Biol. 204*, 191–204.

Barnette, M. S., Daly, P., & Weiss, B. (1983) *Biochem. Pharmacol. 32*, 2929–2933.

Comte, M., Maulet, Y., & Cox, J. A. (1983) *Biochem. J. 209*, 269–272.

Cox, J. A., Comte, M., Fitton, J. E., & Degrado, W. F. (1985) *J. Biol. Chem. 260*, 2527–2534.

Dalgarno, D. C., Klevit, R. E., Levine, B. A., Williams, R. J. P., Dobrowolski, Z., & Drabikowski, W. (1984) *Eur. J. Biochem. 138*, 281–289.

Debye, P. (1915) *Ann. Phys. 46*, 809–823.

Drabikowski, W., Brzeska, H., & Venyaminov, S. Yu. (1982) *J. Biol. Chem. 257*, 11584–11590.

Glatter, O., & Kratky, O. (1982) in *Small Angle X-ray Scattering*, p 150 and pp 157–161, Academic Press, London.

Goldstein, H. (1962) in *Classical Mechanics*, pp 149–151, Addison-Wesley, Reading, MA.

Guinier, A., & Fournet, G. (1955) in *Small-Angle Scattering of X-rays*, p 19, pp 24–28, and pp 135–136, John Wiley & Sons, Inc., New York.

Heidorn, D. B., & Trewhella, J. (1988) *Biochemistry 27*, 909–915.

Heidorn, D. B., Seeger, P. A., Rokop, S. E., Blumenthal, D. K., Means, A. R., Crespi, H., & Trewhella, J. (1989) *Biochemistry 28*, 6757–6764.

Higashijima, T., Wakamatsu, K., Takemitsu, M., Fujino, M., Nakajima, T., & Miyazawa, T. (1983) *FEBS Lett. 152*, 227–230.

Ikura, M., Hiraoki, T., Hikichi, K., Minowa, O., Yamaguchi, H., Yazawa, M., & Yagi, K. (1984) *Biochemistry 23*, 3124–3128.

Izumi, Y., Yoshino, H., Matsuo, T., Matsushima, N., Ueki, T., Kobayashi, K., & Miyake, Y. (1988) *Rep. Prog. Polym. Phys. Jpn. 31*, 571–574.

Izumi, Y., Matsushima, N., & Yoshino, H. (1989) *J. Jpn. Soc. Synchrotron Radiat. Res. 2-1*, 23–33 (in Japanese).

Izumi, Y., Matsushima, N., & Yoshino, H. (1990) The 3rd International Conference on Biophysics and Synchrotron Radiation, Stanford University, Stanford, CA, July 2–6, pp 18–20.

Kataoka, M., Head, J. F., Seaton, B. A., & Engelman, D. M. (1989) *Proc. Natl. Acad. Sci. U.S.A. 86*, 6944–6948.

Klevitt, R. E., Dalgarno, D. C., Levine, B. A., & Williams, R. J. P. (1984) *Eur. J. Biochem. 149*, 109–114.

Lowry, O. H., Rosebrough, N. J., Farr, A. L., & Randall, R. J. (1951) *J. Biol. Chem. 149*, 109–114.

Malencik, D. A., & Anderson, S. R. (1983) *Biochem. Biophys. Res. Commun. 114*, 50–56.

Malencik, D. A., & Anderson, S. R. (1984) *Biochemistry 23*, 2420–2428.

Matsushima, N., Izumi, Y., Matsuo, T., Yoshino, H., Ueki, T., & Miyake, Y. (1989) *J. Biochem. (Tokyo) 105*, 883–887.

Maulet, Y., & Cox, J. A. (1983) *Biochemistry 22*, 5680–5686.

McDowell, L. M., Sanyal, G., & Prenderast, F. G. (1985) *Biochemistry 24*, 2979–2984.

Minowa, O., & Yagi, K. (1984) *J. Biochem. (Tokyo) 96*, 1175–1182.

Persechini, A., & Kretsinger, R. H. (1988) *J. Cardiovasc. Pharmacol. 12 (Suppl. 5)*, S1–S12.

Sanyal, G., Richard, L. M., Carraway, K. L., III, & Puett, D. (1988) *Biochemistry 27*, 6229–6236.

Strynadka, N. C. J., & James, M. N. G. (1990) *Proteins: Struct., Funct., Genet. 7*, 234–248.

Ueki, T., Hiragi, Y., Izumi, Y., Tagawa, H., Kataoka, M., Muroga, Y., Matsushita, T., & Amemiya, Y. (1983) KEK Progress Reports 83-1, Photon Factory Activity Report, 1982/1983, VI-70–VI-71.

Yazawa, M., Sakuma, T., & Yagi, K. (1980) *J. Biochem. (Tokyo) 87*, 1313–1320.

Yoshino, H., Minari, O., Matsushima, N., Ueki, T., Miyake, Y., Matsuo, T., & Izumi, Y. (1989) *J. Biol. Chem. 264*, 19706–19709.